Corrosion Science 184, (2021), 109377
https://doi.org/10.1016/j.corsci.2021.109377
Accepted 6 March 2021

Influence of pressure on the oxidation resistance of carbon fiber reinforced ZrB_2/SiC composites at 2000 and 2200 °C

Antonio Vinci
CNR-ISTEC, Institute of Science and Technology for Ceramics, Via Granarolo 64, I-48018 Faenza, Italy
antonio.vinci@istec.cnr.it

Thomas Reimer
Deutsches Zentrum für Luft- und Raumfahrt e.V. (DLR), Institut für Bauweisen und Strukturtechnologie (BT), Pfaffenwaldring 38-40, 70569 Stuttgart
Thomas.reimer@dlr.de

Luca Zoli
CNR-ISTEC, Institute of Science and Technology for Ceramics, Via Granarolo 64, I-48018 Faenza, Italy
luca.zoli@istec.cnr.it

Diletta Sciti
CNR-ISTEC, Institute of Science and Technology for Ceramics, Via Granarolo 64, I-48018 Faenza, Italy
Diletta.sciti@istec.cnr.it

Abstract

The influence of pressure on the oxidation resistance of C-ZrB_2/SiC composites was studied. Materials were tested in air at 2000-2200 °C at 1-900 mbar. SEM analysis on the tested samples revealed the formation of an outer compact layer of ZrO_2 and an intermediate layer of ZrO_2-SiO_2 as well as a porous interface layer of ZrO_2. SiC increase was beneficial up to 1650 °C, then the trend was inverted. At 1mbar all samples were visibly less damaged and displayed similar performance both at 2000 and 2200 °C, indicating that oxidation resistance is mostly dominated by fiber consumption, which is more severe at ambient pressure.

Keywords

Ceramic-Matrix Composites (CMCs); Ultra-High-Temperature-Ceramics (UHTCs); Oxidation Resistance; Microstructure; Pressure;

1. Introduction

There is increasing demand for materials able to survive extreme conditions, such as those of re-entry in earth's atmosphere, hypersonic flight and propulsion. This led many researchers to study a new class of materials called UHTCMCs (Ultra-high temperature ceramic matrix composites) capable of surpassing the current limitations of C/C and C/SiC composites [1]. These are CMCs where the matrix is constituted by ultra-high temperature ceramic (UHTC) phases. UHTCs are materials with melting points above 3000 °C and are mainly constituted by the carbides and borides of early transition metals, such as HfC, ZrB_2, TaB_2, etc. They are characterized by high thermal conductivities and high temperature strength [2][3][4]. Among UHTCs, ZrB_2 gained growing interest for the fabrication of reusable thermal barriers for aerospace or hypersonic applications [5][6] because of its high thermal conductivity and lower density than hafnium and tantalum compounds [2][7][8].

The main drawback of these materials is the low damage tolerance and thermal shock resistance, so a fiber reinforcement was introduced to overcome these issues [9]. ZrB_2 oxidation resistance is low at temperatures above 1200 °C because of the evolution of volatile oxides (B_2O_3) and the formation of a non-passivating, porous ZrO_2 [10]. The addition of silicides, such as SiC or $MoSi_2$, aids the sintering of ZrB_2 and helps to increase its oxidation resistance by forming a viscous borosilicate glass with low vapour pressure [11][12][13][14]. The oxide layer structure observed in bulk ZrB_2/SiC materials tested in the range of temperatures between 1500 – 1800 °C is mainly constituted by an outer SiO_2 layer, an intermediate ZrO_2 – SiO_2 layer and a SiC depleted zone in the ZrB_2 bulk [15][16][17]. When carbon enters the picture, either in the form of particles or fibers, an additional oxidation phenomenon takes place which is related to the fiber oxidation that starts already at 500 °C. In literature there are several works concerning the oxidation behavior of UHTCs doped with small carbon particles [18][19][20][21], but when it comes to continuous fiber reinforced UHTCs, where the anisotropy of the fibers coupled with the different layer configuration come into play, there is little data. In the framework of the C^3HARME project, this class of materials has been thoroughly characterized in order to understand whether these materials would have been proven valid for the above mentioned applications. Preliminary studies have shown that ZrB_2/SiC based UHTCMCs possess the mechanical resistance required for aerospace applications [22], and recent studies on the oxidation kinetics and behavior of these materials have demonstrated that up to 1650 °C the oxidation resistance is guaranteed by formation of an outer silica glass that protects the material from further oxygen diffusion inside the material [14][23][24]. From the last of these series of studies, it was also concluded that increasing the SiC content from 5 to 20% was beneficial and led to an increase in the oxidation resistance as evidenced from the reduced oxide thickness. Since the main goal is to obtain materials that can withstand temperatures above 2000 °C, further tests are needed. Moreover, the active oxidation of SiC-containing ceramics which is promoted at low oxygen pressures and high temperature remains a major concern and currently there are no

works on the oxidation resistance at ultra-high temperatures or low oxygen pressure of UHTCMCs [25]. The only works that can be found in literature have been done on bulk ceramics with SiC contents above 20 vol% [26][16][27][28]. However, the UHTCMCs previously studied have significant differences from the corresponding bulk materials: the main aspect is the fiber reinforcement that roughly constitutes 50% of the composite. Moreover the amount of readily available SiC is often below 10%. The most recent works on testing of UHTCMCs have validated these materials for the use as thermal barriers in extreme environments such as those encountered in an arc-jet testing facilities, but a lot remains unknown about the oxidation mechanisms and what is more beneficial or detrimental to the oxidation resistance [29].

The objective of this work is to expand and continue our previous work on the oxidation resistance of C-ZrB_2/SiC composites [24] and investigate higher temperature regimes and how the atmospheric pressure influences the oxidation phenomena.

A quick and efficient tool often used to test the oxidation resistance at high temperatures is provided by oxyacetylene torch tests [30][28][31][32][33]. However, the difficulty in controlling and measuring the temperature, together with the temperature gradients, the local oxidation phenomena, and the impossibility of adjusting the atmosphere pressure drove us to research an alternative method to study the oxidation behavior. In order to provide a more controlled environment, an induction-heated facility, named Indutherm, was employed. The materials were tested at 2000 and 2200 °C and at two different pressure regimes and the results were compared with the previous findings.

2. Experimental

2.1. Materials and processing

The composites tested in this work were part of the same batch of fresh material that was also previously tested at 1500 and 1650 °C and were produced by slurry infiltration and hot pressing at 1900 °C. The details pertaining the process, raw powders and production of these materials have been extensively covered in our previous works [34][24]. The four compositions investigated in this paper were reinforced with ~ 40 vol% pitch-based carbon fibers, while the ceramic matrix composition consisted of ZrB_2 doped with SiC in amounts ranging from 5 to 20 vol%, which were labelled as ZS5, ZS10, ZS15 and ZS20.

2.2. Microstructure analysis

Field emission scanning electron microscopy (FE-SEM, Carl Zeiss Sigma NTS Gmbh Öberkochen, Germany) coupled with an energy dispersive x-ray spectroscopy probe (EDS, INCA Energy 300, Oxford instruments, UK) were used to analyse the microstructure and phase composition. Microscopy specimens were prepared by polishing cross sections of the specimens down to a 0.25 μm finish with a semi-automatic polishing machine (Tegramin-25, Struers, Italy). The polished samples were then washed with ethanol in an ultrasonic bath, dried under IR light and cleaned with a plasma cleaner (Colibrì Plasma RF 50 KHz, Gambetti, Italy) at 50 W for 3 min. For the oxidized samples, a thin carbon coating was applied with a turbo-

pumped sputter coater (Q150T, Quorum Technologies Ltd, UK) on the surface of the specimens to avoid electron scattering on the oxides layers during SEM analysis. The theoretical density is calculated with the formula reported below:

$\rho = f_{matrix} \times \rho_{matrix} + f_{fiber} \times \rho_{fiber}$

where f is the volumetric fraction of the matrix and fibers respectively (which are measured by image analysis). The relative density is then obtained as the ratio between the actually measured density and this theoretical density.

The fiber volumetric amount was measured by image analysis using the software Image-Pro Analyser 7.0 (standard ISO 13383-1, method A2). X-Ray diffraction analysis was carried out on the samples oxidized at 2000 and 2200 °C at 1 - 900 mbar, using a Bruker D8 Advance apparatus (Bruker, Karlsruhe, Germany). Thermodynamic calculations were carried out with software Factsage 7.0 to predict the most stable phases potentially formed at high temperatures and correlate these simulations to the phases experimentally observed.

2.3. Oxidation test setup

Specimens with dimensions 2.5 × 2×12.5 mm (Width × Thickness × Length) were machined from the sintered pellet. The samples were cleaned with ethanol and dried at 100 °C in an oven. The oxidation tests were performed in the Indutherm facility, an inductively heated mechanical test bench that was customized and equipped with a homemade testing chamber made of porous zirconia boards (Zirconia 76 % porosity, density 1.4 g/cm^3, Zircar Zirconia, Florida, NY 10921-0287) (Fig. 1). This facility is constituted by an outer metal chamber with water-cooled walls, hermetically sealed, equipped with a vacuum pump system that can operate in a range of pressures from below 1 mbar to ambient pressure. The zirconia chamber is equipped with a graphite plate as the top cover, which is inductively heated by a copper coil. The temperature inside the chamber is monitored through the use of a 2-color measurements/quotient-pyrometer, (temperature range 800-2400°C, model PZ40 AF4, 0/4-20mA (RS232) Keller, Germany) that points directly at the sample holder (also made of zirconia) through a small hole in the front wall of the chamber. The gas enters the chamber through a zirconia tube inserted in a hole present on the right wall, and exits through holes on the left wall. This chamber is placed inside the Indutherm, on top of an insulated support. The chamber is also surrounded by porous graphite plates.

The specimens are placed on a sample holder, which is then introduced in the zirconia chamber. The holder was made of microporous zirconia and the edges of the holder were bevelled into a V shape to minimize surface area contact and limit reactions with the specimens. The Indutherm is sealed and evacuated down to a pressure of 5 mbar, then flushed with Argon twice. Then the pressure is set to either 1 mbar or 900 mbar (closest pressure to ambient pressure) and the chamber is heated to the target temperature (2000 or 2200 °C) at a rate of 100 °C/min. Once the temperature is reached, air flows in the refractory chamber at a flow rate of 5 l/min for 2 min. After 2 min, the air inlet is closed and the chamber is cooled down naturally. The exposure

times have been decided taking into account the operating times at extreme conditions typically encountered in aerospace applications (30-60s) [35]. Samples were weighed before (w_{in}) and after (w_{fin}) oxidation cycles and the weight difference was calculated and normalized over the initial surface area (S):

$$\frac{\Delta w}{S} = \frac{w_{fin} - w_{in}}{S}$$

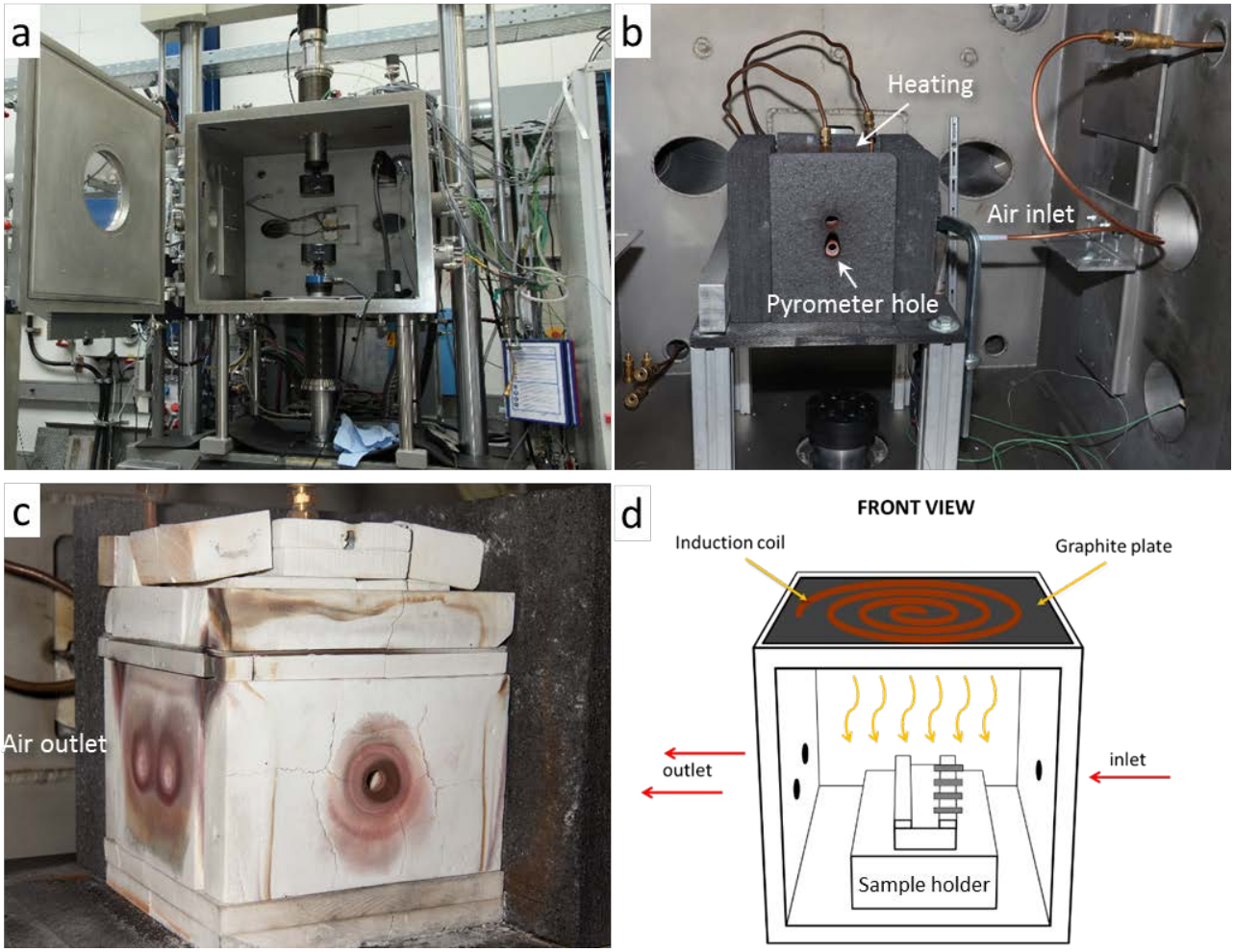

Figure 1. a) Indutherm facility constituted by an outer steel chamber and a vacuum pump system regulated from a console. b) Exterior of the oxidation chamber used for testing constituted by porous graphite walls and an inner zirconia chamber, c) Inner zirconia chamber , d) Schematic of the chamber: the heating is provided by a graphite plate used as the top cover of the chamber and heated by an induction coil. Holes are present on the side walls to allow for the inlet and outlet of gas. The pyrometer points at the sample holder through a hole in the front wall.

3. Results and discussion

3.1 Microstructure of the sintered material

The features of these composites have been thoroughly described in our previous papers [34][24] and are summarized in table 1, while the typical microstructure of these materials is shown in figure 2.

Table 1. Physical and mechanical properties of samples ZS5, ZS10, ZS15, ZS20 produced in our previous works via slurry infiltration and hot pressing at 1900 °C, 40 MPa for 15min. Flexural strength and fracture toughness were evaluated by 4-point bending tests.

Sample	$\rho_{experim}$ (g/cm^3)	ρ_{theor} (g/cm^3)	ρ_{rel} (%)	porosity (vol%)	fiber (vol%)	σ (MPa)	K_{Ic} ($MPa \cdot m^{0.5}$)	Reference
ZS5	3.65	4.19	87.1	12.9	40	198 ± 12	4.8 ± 0.3	[34][24]
ZS10	3.86	4.28	90.2	9.8	38	196 ± 28	6.1 ± 0.3	[34][24]
ZS15	3.95	4.27	92.5	7.5	37	186 ± 49	6.3 ± 0.4	[34][24]
ZS20	4.00	4.23	94.6	5.4	37	164 ± 2	5.0 ± 0.9	[34][24]

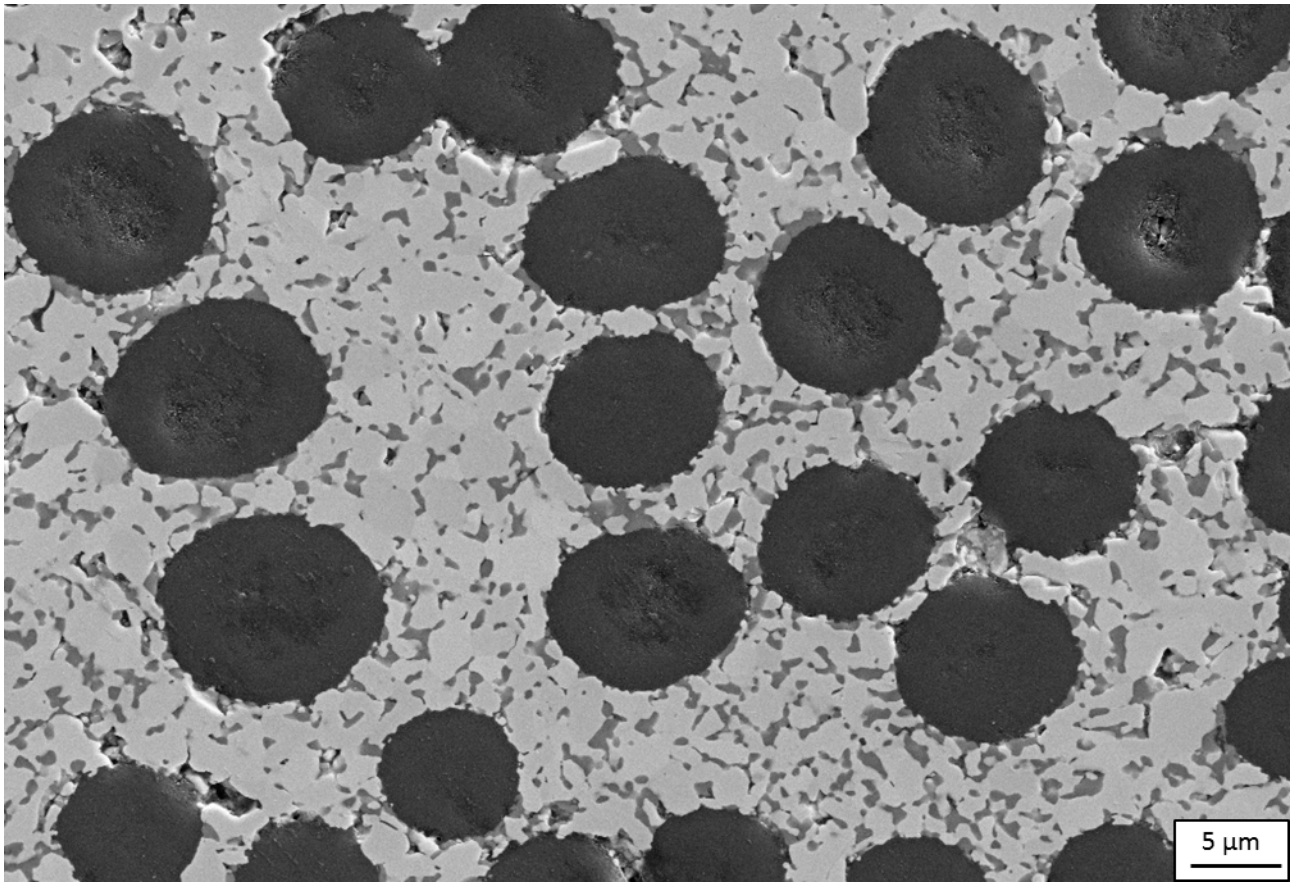

Figure 2. Microstructure of sample ZS15 taken as reference showing the typical fiber distribution. The fibers are in black, while light and dark grey represent ZrB_2 and SiC respectively.

The fibers and SiC particles were homogeneously distributed in the ceramic matrix and the interface between the fibers and SiC was relatively strong due to the reaction of the surface oxides of SiC particles with the fibers to form SiC via carbo-thermal reduction (fig. 2) [36]. The relative density increased with increasing the SiC content owing to the capability of SiC to aid the sintering of ZrB_2 via liquid phase sintering (table 1) [37][38]. In all samples the fibers were not excessively consumed by the oxide impurities present in the ceramic matrix and maintained their original shape, in agreement with the works on fiber reactivity by Silvestroni et al. [39].

3.2 Oxidation tests at 2000 and 2200 °C at 900 mbar

All samples underwent weight loss after oxidation at 2000 °C both at 1 and 900 mbar. The lack of a clear trend among the specimens tested in the same conditions could be attributed to slight variations in the fiber contents which are typical of this process. The samples tested at a pressure of 900 mbar were characterized by mass losses in the range of 160-210 mg/cm^2, while the samples tested at 1 mbar were considerably lower, in the range of 100-130 mg/cm^2, highlighting the influence of pressure. Further mass loss was incurred at 2200 °C likely due to a higher degree of oxidation, but the difference was within 15% of the mass loss at 2000 °C, suggesting that further increasing the temperature did not affect the materials' oxidation resistance as much as the pressure did. From a rough estimation, the specific mass loss rate normalized on the timescale of interest (2 min) amounts to 8 – 16 g/m^{2}s for the composites investigated.

Table 2. Mass variation normalized on the surface area after oxidation tests at 2000 and 2200 °C, and at pressures of 1-900 mbar for samples ZS5, ZS10, ZS15 and ZS20.

	Δw/S (mg/cm^2)			
Sample	**1 mbar**		**900 mbar**	
	2000 °C	**2200 °C**	**2000 °C**	**2200 °C**
ZS5	- 105	- 121	- 161	- 197
ZS10	- 115	- 128	- 171	- 212
ZS15	- 120	- 137	- 169	- 211
ZS20	- 118	- 135	- 165	- 194

XRD analysis was carried out on all samples after testing at 2000 and 2200°C at 900 mbar, but the only identified phase was monoclinic ZrO_2 (PDF#86-1449) and occasionally some peaks related to $CaCO_3$ coming from the supporting clay used in the sample holder. No cubic or tetragonal zirconia was identified in any condition and the only difference observed was the peak intensity going from 2000 to 2200 °C

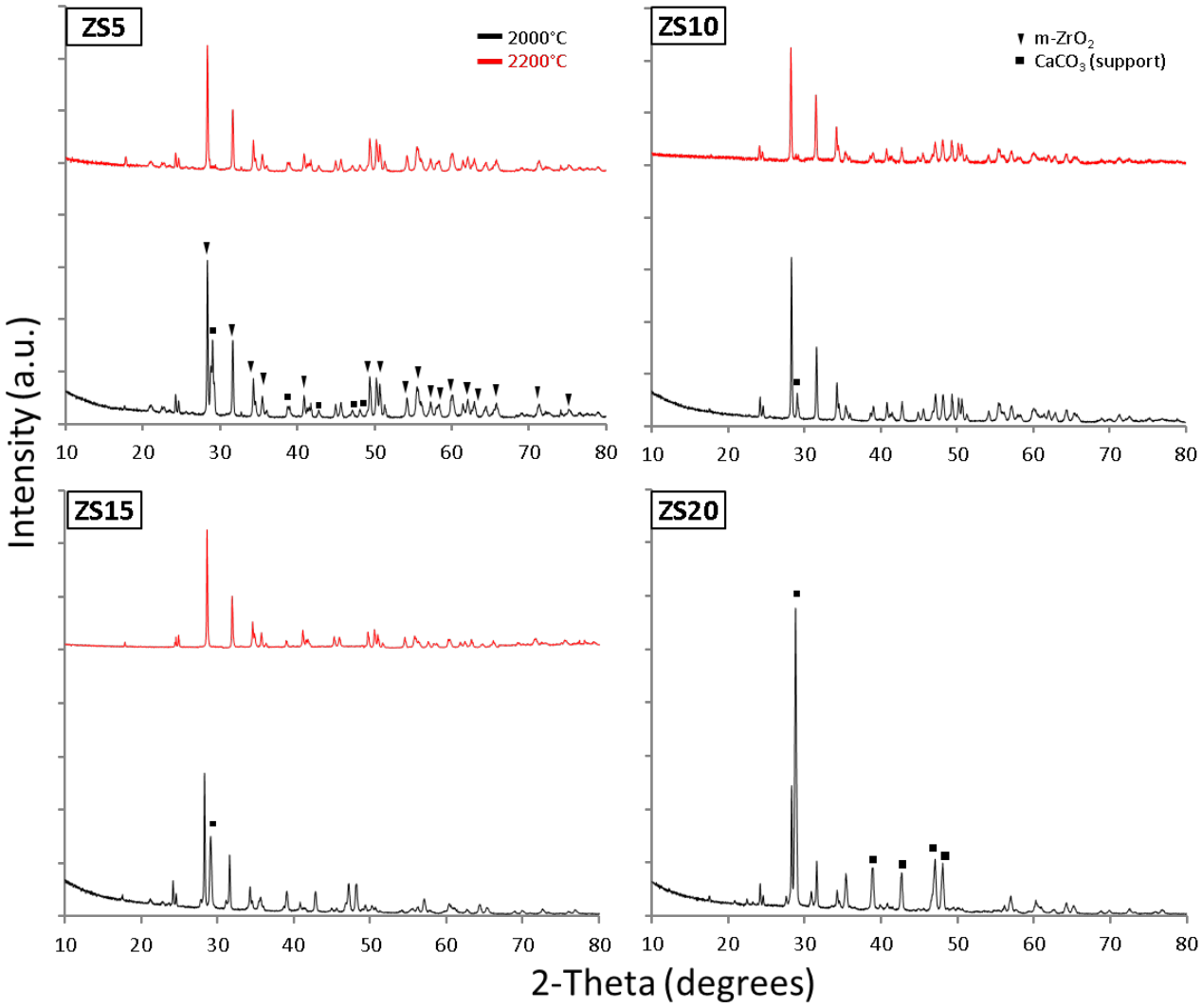

Figure 3. XRD pattern of sample ZS5, ZS10, ZS15 and ZS20 after testing at 2000 and 2200 °C at 900 mbar. All peaks are relative to monoclinic zirconia. The extra peaks that can be found occasionally are due to calcite peaks originating from the supporting clay used in the sample holder. In the case of ZS20 tested at 2200°C and 900 mbar it was not possible to obtain any spectra due to the excessively damaged oxide scale.

In fig. 4, the high magnification micrographs of the surface, cross section and detail of samples ZS5-20 oxidized at 2000 °C at a pressure of 900 mbar is shown. The white and dark grey phases represent ZrO_2 and SiO_2 respectively as ascertained by EDS, while the black dots are the hollows left by the carbon fiber oxidation. The peak belonging to carbon, present in most spectra, arises from the carbon coating of the carbon sputter.

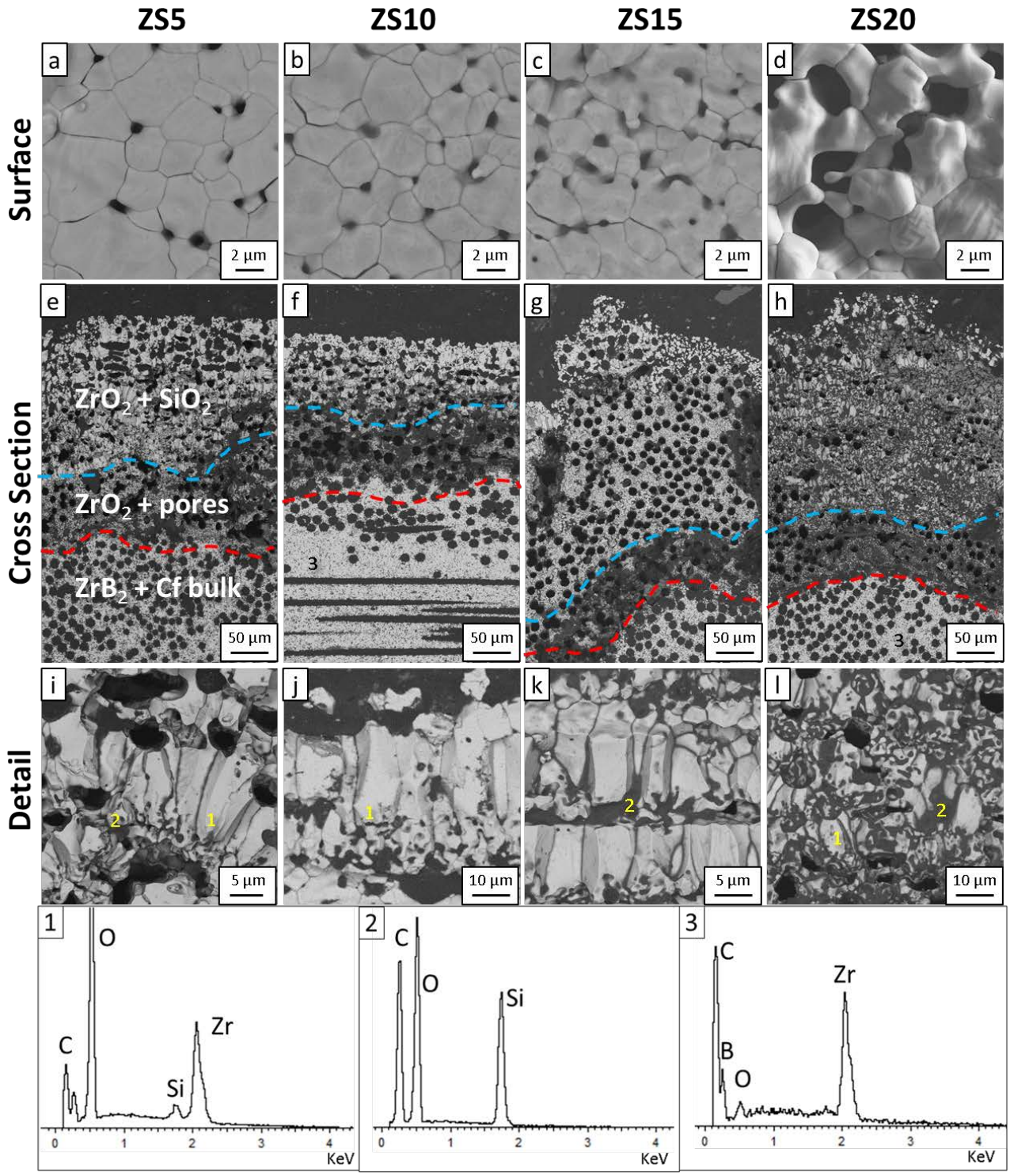

Figure 4. Micrographs of ZS5, ZS10, ZS15 and ZS20 after testing at 2000 °C and 900 mbar: a,b,c,d) Surface layer of ZrO_2 with the pores left by SiC removal, e,f,g,h) Cross section showing the oxide scale stratification: outer coarse ZrO_2 layer with traces of SiO_2, intermediate porous ZrO_2 layer, unreacted bulk, i, j, k, l) Detail of the outer scale, showing large ZrO_2 grains with increasingly higher SiO_2 content. EDS spectra is shown below.

Previously Fahrenholtz *et al.* extensively discussed the formation of a SiC-depleted scale at the interface between the ZrO_2/SiO_2 layer and the unreacted material in a bulk ZrB_2/SiC ceramic, originating from the active oxidation of SiC to SiO [15]. The same author also investigated the influence of graphite

addition in a ZrB_2/SiC composite and found out that the presence of carbon may lead to the preferential formation of CO which lowers the SiO partial pressure and allows to retain the SiC phase [18]. In our previous work on the oxidation resistance of these materials up to 1650 °C, no SiC-depleted layer was observed and the layers identified were an outer scale of SiO_2, an intermediate layer of ZrO_2 and SiO_2 with some hollows left by the carbon fiber oxidation, and the unreacted bulk.

In the present study, the surface of all specimens was characterized by a compact layer of large ZrO_2 grains and pores that grew in size and number with the increase of SiC content (fig 4, a,b,c,d). These were attributed to the oxidation of SiC particles to SiO and SiO_2 that were removed from the surface, leaving behind an increasing number of pores with the increase of SiC. From the micrographs on the cross sections of the oxidized specimens, two main layers could be identified: 1) an outer scale which consisted mostly of coarse ZrO_2 grains with traces of silica between the grains for samples ZS5, ZS10 and ZS15 (fig 4, e, f, g); for sample ZS20 (fig. 4 h), smaller ZrO_2 grains and a higher amount of SiO_2 were observed. This last specimen was also the most friable during machining and the majority of the oxide layer was lost, suggesting that high amounts of SiC do not allow for the formation of a compact layer during oxidation. 2) a porous intermediate layer of fine ZrO_2 grains and the hollows left by the fiber oxidation. While for the outer layer a portion of the fiber hollows was either filled with SiO_2 or collapsed and sintered to form a compact ZrO_2 layer, in the case of this intermediate layer the structure formed by the fine ZrO_2 grains represented the weakest point and this was reflected in the difficulty encountered during the polishing of the cross-sections due to the tendency of this layer to crumble, leading to the detachment of the entire oxide layer.

After testing at 2200 °C and 900 mbar, the samples were visibly more damaged and fragile. The oxide layer was very prone to detachment and polishing was extremely difficult and in some cases impossible.

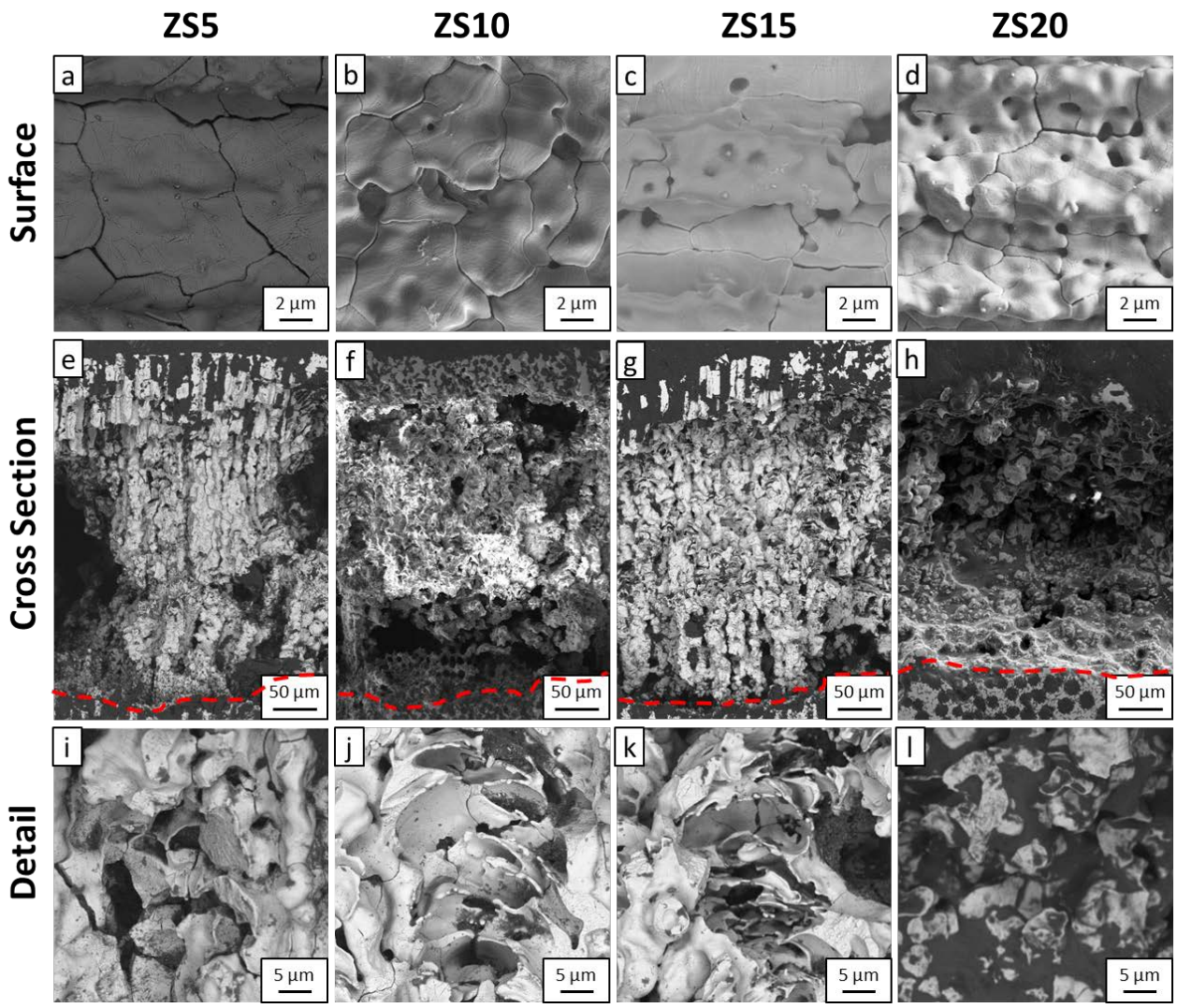

Figure 5. Micrographs of ZS5, ZS10, ZS15 and ZS20 after testing at 2200 °C and 900 mbar: a,b,c,d) Surface layer of ZrO_2 with the pores left by SiC removal, e,f,g,h) Cross section showing the oxide scale stratification: in this case, only a continuous ZrO_2 layer with traces of SiO_2 was observed, followed by the unreacted bulk, i, j, k, l) Detail of the outer layer, showing the hollows left by the violent evolution and bubbling of volatile oxides.

Like for the specimens tested at 2000 °C and 900 mbar, the surface of all specimens was comprised of a compact layer of large ZrO_2 grains. Pores deriving from SiC oxidation were still present but the majority was closed by the sintering of the outer layer (fig 5, a,b,c,d) and no significant difference was observed across the four specimens. Looking at the cross sections of the tested samples (above the red line), only a continuous layer of large columnar ZrO_2 grains with traces of SiO_2 was observed, while the hollows left by the carbon fibers were no longer recognizable. This layer was more impoverished of SiO_2 compared to the one observed at 2000 °C and it was very fragile and prone to crumbling during polishing. The porous intermediate layer between the outer scale and the unreacted bulk previously observed at 2000 °C was not seen at 2200 °C. On closer inspection of the oxide scale microstructure (fig. 5, i, j, k) large voids were observed; these were attributed to the violent bubbling of the liquid phase, namely $SiO\text{-}B_2O_3$, and the

oxidation of the fibers with the formation of CO, that burst through the sample. For sample ZS20 (fig. 5, l) SiO_2 was still present and abundant between the ZrO_2 grains, indicating that not all the SiO_2 evaporated from the specimen. Once again, just like at 2000 °C, this specimen was also characterized by the weakest oxide layer that was very prone to detachment.

The oxide layer thickness was irregular across all the specimens, a phenomenon that was previously observed by Opila and which is characteristic of these composites [40]. The thicknesses of the oxidized layers for samples ZS5-20 after testing at 2000 and 2200 °C at 900 and 1 mbar is reported in table 3 and is compared with the results obtained in our previous paper where specimens of the same batch were tested at 1500 and 1650 °C. The reported values are the average thickness measured on all the four sides of the specimens (3 measurements per side).

Table 3. Oxide layer thickness of samples ZS5, ZS10, ZS15 and ZS20 after testing in air at pressures of 1 – 900 mbar at 2000 and 2200 °C, compared with specimens tested at 1500 and 1650 °C in air at ambient. For sample ZS20 tested at 2200 °C, a portion of the outer layer was detached, therefore the reported thickness underestimates the real oxide thickness.

Sample	Pressure (mbar)	Oxide layer thickness (μm)			
		1500 °C	1650 °C	2000 °C	2200 °C
ZS5	900	64 ± 5	85 ± 12	317 ± 31	388 ± 25
	1			127 ± 13	120 + 18
ZS10	900	50 ± 6	57 ± 5	295 ± 45	375 ± 38
	1			121 ± 9	134 ± 14
ZS15	900	45 ± 5	50 ± 11	365 ± 30	413 ± 44
	1			113 ± 21	157 ± 21
ZS20	900	36 ± 8	35 ± 4	382 ± 17	425 ± 66
	1			123 ± 20	169 ± 10

Between 1500 and 1650 °C, the increase of SiC content led to a progressively thinner oxide layer due to the formation of a protective borosilicate layer which prevented further oxidation. Higher SiC content provided higher amounts of the protective layer, leading to an increase of the oxidation resistance with the increase of SiC up to 1650 °C. Between 2000 and 2200 °C this trend is reversed; the borosilicate layer no longer provides protection and readily evaporates from the surface, leaving behind an increasing number of voids. In this case, higher SiC contents led to a higher number of pores and voids in the microstructure, therefore decreasing the oxidation resistance and the overall oxide scale structure stability. Sample ZS10 is characterized by the lowest oxide thickness at 2000 °C, even though at 2200 °C the thickness value is closer to the other specimens. Sample ZS5 contains the lowest amount of SiC, its oxidation resistance is inferior up

to 1650 °C. This was attributed to the low amount of protective borosilicate layer formed on the surface. At 2000 and 2200 °C its oxidation is still poor or comparable to the higher SiC-containing samples. This was attributed to the insufficient amount of liquid phase between the grains responsible for keeping the scale together. Samples ZS15-20 contain the highest amount of SiC which is reflected in the superior oxidation resistance up to 1650 °C. At 2000 and 2200 °C this effect is reversed and a high amount of liquid phase in the oxide scale is actually detrimental (as for sample ZS20). ZS10 seems to strike the optimal balance between ZrB_2 and SiC, resulting in the overall best compromise.

3.3 Oxidation tests at 2000 and 2200 °C at 1 mbar

The oxide layer thickness of the specimens tested at 2000 and 2200 °C at 1 mbar is reported in Table 4 and compared to the specimens tested at 900 mbar. The lower mass loss compared to the specimens tested at 900 mbar (Table 2) was reflected in the lower oxide layer thickness, which is in the range of 110-170 µm, almost three times less than the samples tested at 900 mbar (table 3). From the XRD spectra of the sample tested at 2000-2200 °C at 1 mbar, only monoclinic zirconia was observed again just like at 900 mbar, with slight variations in intensity going from 2000 to 2200 °C. As mentioned before, the extra peaks observed at 29, 37, 43, 47 and 49 2-theta belong to the calcite present in the supporting clay used in the sample holder.

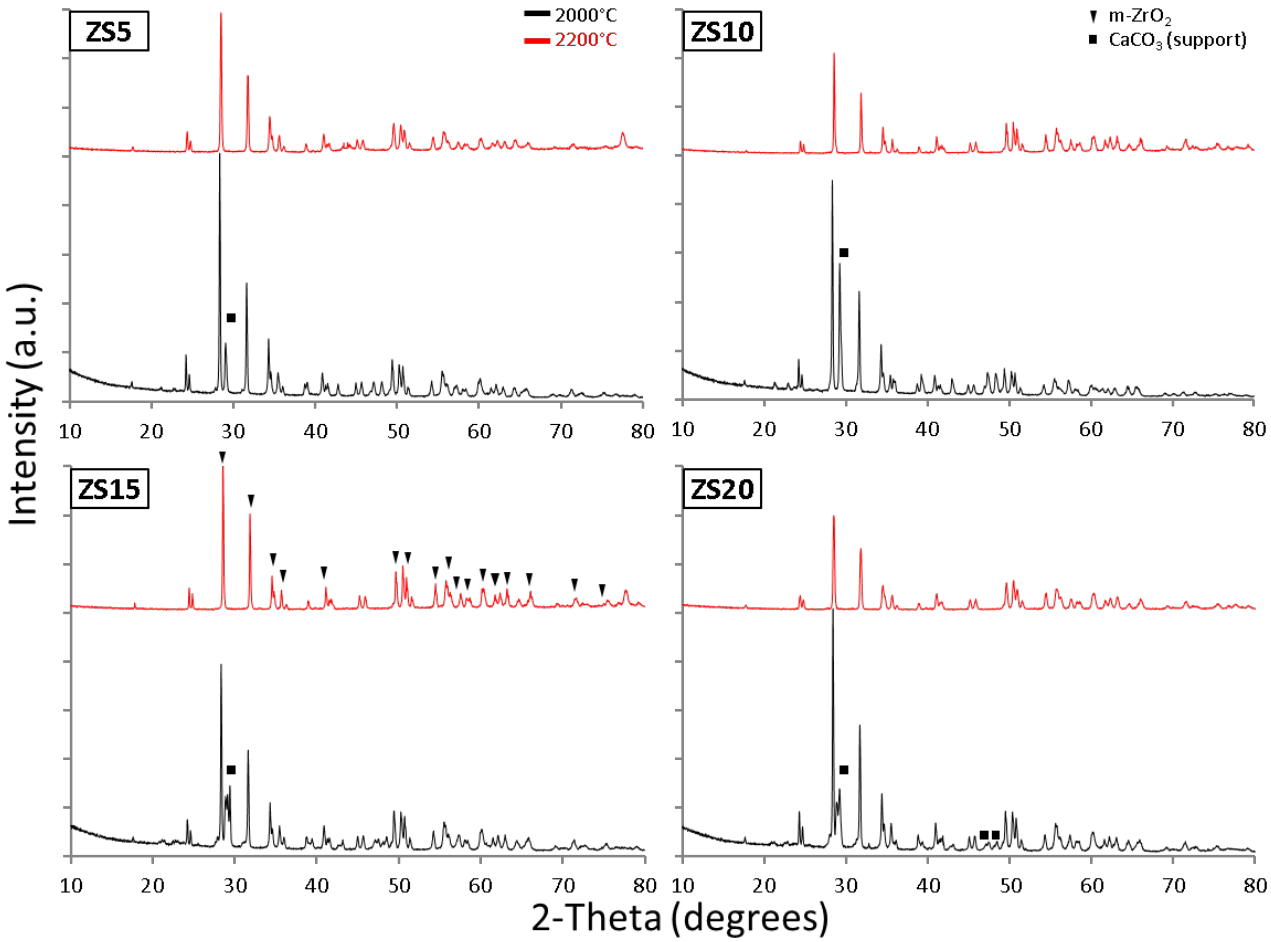

Figure 6. XRD pattern of sample ZS5, ZS10, ZS15 and ZS20 after testing at 2000 and 2200 °C at 1 mbar. All peaks are relative to monoclinic zirconia. The extra peaks that can be found occasionally are due to calcite peaks originating from the supporting clay used in the sample holder.

In fig. 7, the high magnification micrographs of the surface and cross section of samples ZS5-20 oxidized at 2000 °C at a pressure of 1 mbar is shown.

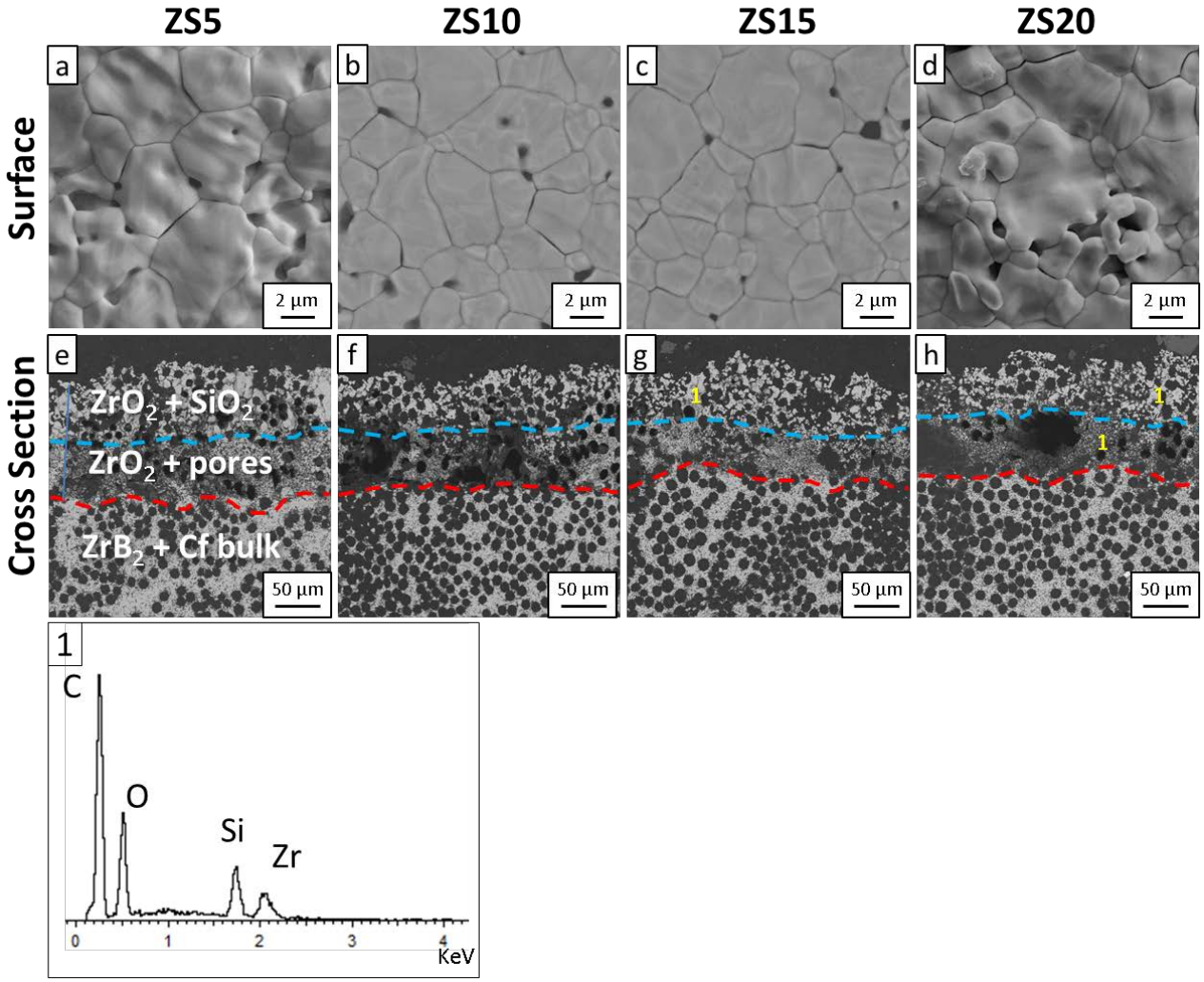

Figure 7. Micrographs of ZS5, ZS10, ZS15 and ZS20 after testing at 2000 °C and 1 mbar: a,b,c,d) Surface layer of ZrO_2 with the pores left by SiC removal, e,f,g,h) Cross section showing the oxide scale stratification: outer ZrO_2 layer with traces of SiO_2, intermediate ZrO_2 layer with the hollows left by carbon fiber oxidation, unreacted bulk. Below the EDS spectra.

The surface of the samples tested at 2000 °C, at 1 mbar closely resembles that observed at 900 mbar: the surface is comprised by ZrO_2 grains with the presence of small pores attributed to the removal of SiC from the surface (fig. 7, a, b, c and d). The cross section highlights the same layer structure observed before: outer scale of zirconia with traces of SiO_2, an intermediate layer of porous ZrO_2 (fig. 7, e, f, g and h, between the blue and red line), and the unreacted bulk (fig. 7, e, f, g and h, below the red line). Only in sample ZS20 SiO_2

was observed in the intermediate porous layer of ZrO_2 as well. However, unlike the samples tested at 900 mbar, these were visibly less damaged as evidenced by the thinner oxide layer. Moreover the oxide scale was well adhered to the surface and was not prone to detachment, in spite of the presence of the porous weak layer.

At 2200 °C and 1 mbar, the oxide structure was mostly unchanged. The surface layer was always comprised of large ZrO_2 grains and the hollows left by SiC removal which were slightly larger than those observed at 2000 °C (fig. 8, a, b, c and d). In these conditions it was difficult to tell the oxide layers apart and the main layer identified was a porous ZrO_2 layer with the cavities left by fibers removal and almost no SiO_2. Even in this case, the oxide layer was well adhered to the surface in spite of the porous structure.

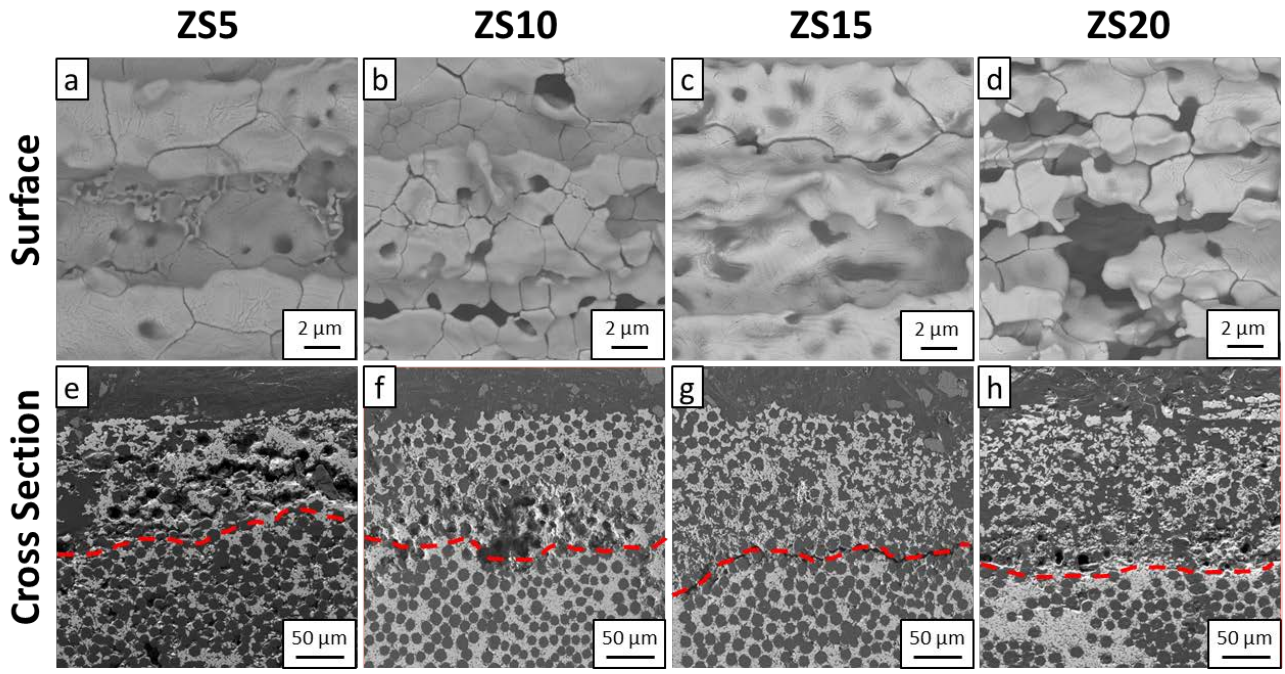

Figure 8. Micrographs of ZS5, ZS10, ZS15 and ZS20 after testing at 2200 °C and 900 mbar: a,b,c,d) Surface layer of ZrO_2 with the pores left by SiC removal, e,f,g,h) Cross section showing the oxide scale stratification: porous ZrO_2 layer with the hollows left by carbon fiber oxidation, unreacted bulk. The dark grey phase observed in the outer scale is not SiO_2 but the resin used to mount the sample that infiltrated the pores.

3.4 Oxidation mechanism

The kinetics of oxidation of ZrB_2/SiC based UHTCMCs composite in the range of temperature from 800 to 1650 °C are mainly characterized by two competing phenomena; 1) weight loss due to the oxidation of the carbon fibers (reactions 1, 2), 2) oxidation of ZrB_2 and SiC to the corresponding oxides (reactions 3,5)

$$C + ½\ O_2 \rightarrow CO_{(g)} \qquad (1)$$

$$C + O_2 \rightarrow CO_{2(g)} \quad (2)$$

$$ZrB_2 + 5O_2 \rightarrow ZrO_{2(s)} + B_2O_{3(l,g)} \quad (3)$$

$$SiC + 3/2O_2 \rightarrow SiO_{2(l)} + CO_{(g)} \quad (4)$$

$$SiC + O_2 \rightarrow SiO_{(g)} + CO_{(g)} \quad (5)$$

Reaction 3 begins at T >800 °C while the formation of borosilicate glass starts at higher temperature (1100 °C). The quicker the formation of the silica layer, the slower is the fiber oxidation [14]. The most critical temperature was found to be 1000 °C, which corresponds to the maximum weight loss, because there is no protective layer on the surface and fibers get rapidly oxidized [14]. At T > 1100 °C, the silica layer is formed and the fibers oxidation is progressively halted up to 1650 °C [24].

Thermodynamic simulations were carried out at 2000 and 2200 °C, from 1 to 1000 mbar, taking into account the mole ratios between the compounds investigated (1 SiC + 2.5 ZrB_2 + 7 C) in the presence of excess oxygen, to monitor how the formation of the volatile species was affected. The diagram at 2200 °C was almost identical to the one at 2000 °C, with a slight shift in all the gases pressures, therefore only the formed will be discussed. At 1 bar, the most thermodynamically stable products were t-ZrO_2 and SiO_2, but only m-ZrO_2 was found from XRD analysis. This was attributed to the lack of a phase that could stabilize t-ZrO_2 at lower temperatures, such as Y_2O_3. $ZrSiO_4$ is not stable past 1600-1700°C and will decompose back to ZrO_2 and SiO_2, which is in agreement with what observed from XRD analysis. The main volatile species in these conditions are CO_2, B_2O_3 and BO_2. A portion of the formed SiO_2 is also predicted to evaporate as $SiO_{2(g)}$. With the decrease of pressure down to 1 mbar, the atmosphere becomes richer in $CO_{(g)}$ and $SiO_{(g)}$, while boron has more tendency to be removed as BO_2. In all cases the majority of oxygen is consumed for the oxidation of the fibers.

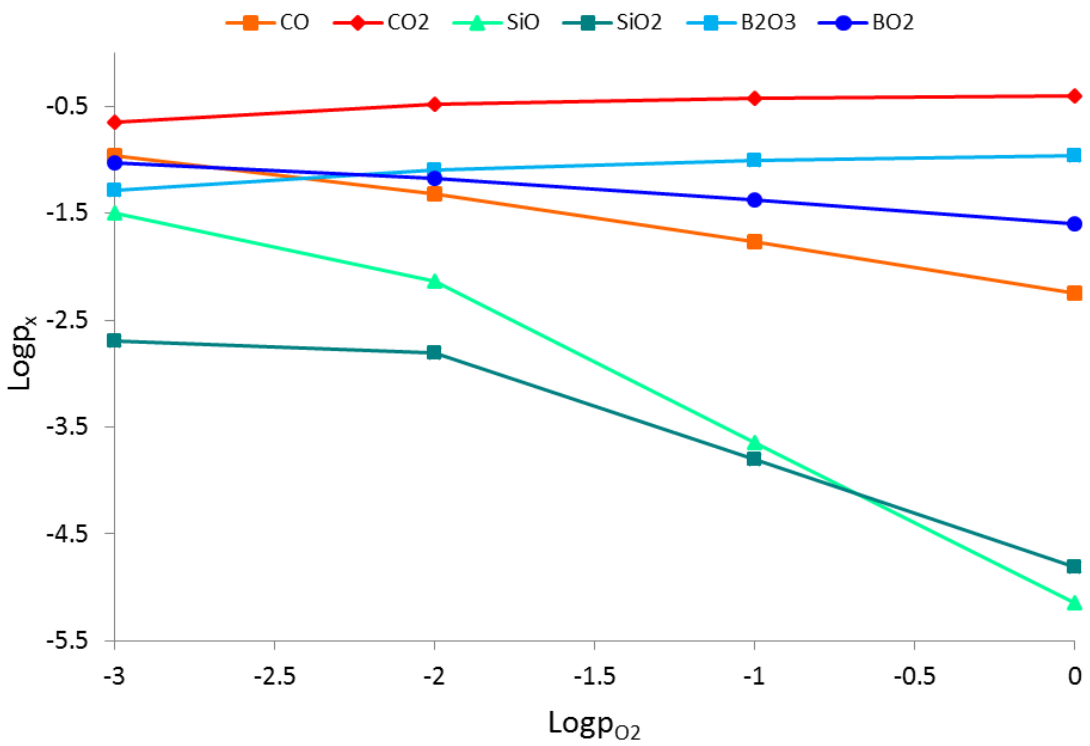

Fig. 9 Variation of volatile species partial pressures with the decrease of oxygen partial pressure. At ambient pressure, the main species are CO_2, B_2O_3 and BO_2, while with the decrease of oxygen pressure, SiO and CO become more abundant.

From these simulations, the following oxidation mechanism was hypothesized: with exposure at 2000 °C, the majority of the surficial fibers are oxidized to CO_2 and CO. SiC undergoes both active and passive oxidation, and part of the formed silica evaporates. ZrB_2 is oxidized to porous ZrO_2, while boron is removed as B_2O_3 and BO_2. The resulting porous structure leads to further oxygen diffusion inside the composite and oxidation of the inner fibers. Part of the liquid SiO_2 tends to migrate and evaporate, moving through the channels left by the fibers oxidation, while the surficial ZrO_2 grains start growing in size, progressively blocking the channels and trapping any SiO_2 between the grains. This effect was more evident for ZS20 due to the higher SiC content (Fig. 4h). When the temperature is set to 2200 °C, these phenomena are more severe and violent, and the liquid phase, together with CO originating from the carbon oxidation, start bubbling and bursting through the zirconia layer, resulting in a severely damaged scale. The proposed model summarizing these phenomena is illustrated in figure 10: the specimen is initially exposed to air, which leads to the rapid oxidation and removal of the outer fibers, SiC and the B_2O_3 originating from ZrB_2 oxidation. This is followed by the migration and partial evaporation of the inner SiO_2 through the channels left by the fibers removal. Finally the grain growth of ZrO_2 traps the residual SiO_2 and leads to the collapse of fiber hollows, leaving an outer compact scale. At lower pressures these phenomena are less intense and the majority of SiC is converted to SiO.

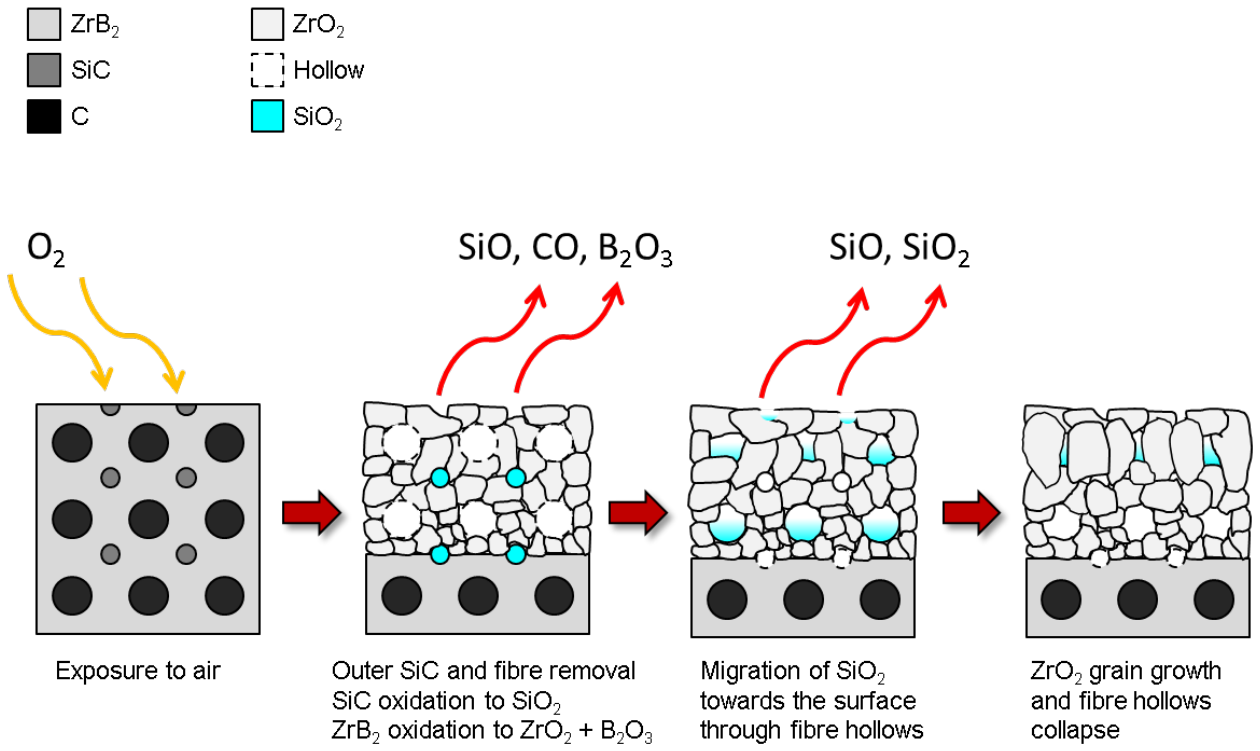

Figure 10. Model for the oxidation mechanism at 2000-2200 °C for a carbon fiber reinforced ZrB_2/SiC composite: 1) exposure to air, 2) oxidation and removal of the outer fibers and SiC as volatile oxides and oxidation of ZrB_2 to ZrO_2 and B_2O_3 which is removed as well, 3) migration of the inner SiO_2 through the fiber hollows and partial evaporation, 4) ZrO_2 grain growth which leads to the collapse of fiber hollows and entrapment of residual SiO_2 along grains.

Bulk ceramics containing SiC are affected by different oxygen partial pressures because at high pressure, SiC turns into SiO_2 which spreads on the surface and provides some passivation, whereas at lower oxygen pressure it turns into volatile SiO, providing no protection and leaving a porous structure. Therefore, in the case of bulk ceramics, a lower oxygen pressure is the most detrimental condition. In the case of fiber reinforced composites, the argument about SiC active oxidation still stands, but the main factor that determines the composite oxidation resistance mostly lies in the oxidation resistance of the fiber reinforcement, which is much more susceptible to oxidation. In this case, SiC active oxidation is only a secondary issue and having a lower oxygen pressure actually results in the least severe oxidation condition for the composite. On the contrary, a higher oxygen pressure promotes the preferential formation of SiO_2 (and therefore lessening this secondary issue), but it also severely speeds up the fiber oxidation, resulting in the most severe oxidation condition. Therefore, the argument concerning SiC detrimental effect on the oxidation resistance of UHTCMCs still stands, but its effects are of little relevance when compared to the fiber oxidation phenomena which are the main reason for the specimen potential failure under oxidizing environment.

Conclusions

The influence of SiC content and pressure on the oxidation resistance in air of fiber reinforced ZrB_2-SiC composites was investigated at 2000 and 2200 °C. The exposure to high temperatures triggers the rapid oxidation of fibers and SiC which are readily removed, while ZrB_2 is oxidized to ZrO_2 and B_2O_3. The temperature is too high for any protective borosilicate layer to form as it usually happens at T < 1650 °C, and the protection to further oxygen penetration is mainly provided by an outer compact layer of large ZrO_2 grains. SiO_2 was only found in traces between the zirconia grains, and at 2200 °C it is obvious how higher SiC contents are actually detrimental for the oxidation resistance in this temperature range due to the violent bubbling of volatile oxides through the zirconia scale that leaves large pores behind.
Comparing samples with different SiC amounts in the same testing conditions, led to the conclusion that increasing SiC is beneficial only up to 1650°C, but that at 2000°C this effect is reversed and lower SiC contents are more beneficial. When it comes to the overall oxidation resistance, low oxygen partial pressures are the least severe conditions because fiber oxidation is the main phenomenon affecting the oxidation resistance. As far as the application potential is concerned, in light of the very high temperature and high oxygen pressure used during the tests, at least for applications with short term duration, the material performs well, with oxide scales on the order of 0.4 mm.

Acknowledgements

This work has received funding from the European Union's Horizon 2020 "Research and innovation programme" under grant agreement N°685594 (C^3HARME).

The raw/processed data required to reproduce these findings cannot be shared at this time due to technical or time limitations.

References

[1] H. Hald, Operational limits for reusable space transportation systems due to physical boundaries of C/SiC materials, Aerosp. Sci. Technol. 7 (2003) 551–559. https://doi.org/10.1016/S1270-9638(03)00054-3.

[2] M.M. Opeka, I.G. Talmy, E.J. Wuchina, J. a. Zaykoski, S.J. Causey, Mechanical, Thermal, and Oxidation Properties of Refractory Hafnium and zirconium Compounds, J. Eur. Ceram. Soc. 19 (1999) 2405–2414. https://doi.org/10.1016/S0955-2219(99)00129-6.

[3] S. Tang, J. Deng, S. Wang, W. Liu, Comparison of thermal and ablation behaviors of C/SiC composites and C/ZrB2-SiC composites, Corros. Sci. 51 (2009) 54–61. https://doi.org/10.1016/j.corsci.2008.09.037.

[4] W.W. Wu, M. Estili, T. Nishimura, G.J. Zhang, Y. Sakka, Machinable ZrB2-SiC-BN composites fabricated by reactive spark plasma sintering, Mater. Sci. Eng. A. 582 (2013) 41–46. https://doi.org/10.1016/j.msea.2013.05.079.

[5] A. Paul, J. Binner, B. Vaidhyanathan, UHTC Composites for Hypersonic Applications, in: Ultra-High Temp. Ceram. Mater. Extrem. Environ. Appl., 2014: pp. 144–166. https://doi.org/10.1002/9781118700853.ch7.

[6] A. Cecere, R. Savino, C. Allouis, F. Monteverde, Heat transfer in ultra-high temperature advanced ceramics under high enthalpy arc-jet conditions, Int. J. Heat Mass Transf. 91 (2015) 747–755. https://doi.org/10.1016/j.ijheatmasstransfer.2015.08.029.

[7] S.R. Levine, E.J. Opila, M.C. Halbig, J.D. Kiser, M. Singh, J.A. Salem, Evaluation of ultra-high temperature ceramics for aeropropulsion use, J. Eur. Ceram. Soc. 22 (2002) 2757–2767. https://doi.org/10.1016/S0955-2219(02)00140-1.

[8] F. Monteverde, S. Guicciardi, A. Bellosi, Advances in microstructure and mechanical properties of zirconium diboride based ceramics, Mater. Sci. Eng. A. 346 (2003) 310–319. https://doi.org/http://dx.doi.org/10.1016/S0921-5093(02)00520-8.

[9] J.J. Sha, J. Li, S.H. Wang, Z.F. Zhang, Y.F. Zu, S. Flauder, W. Krenkel, Improved microstructure and fracture properties of short carbon fiber-toughened ZrB2-based UHTC composites via colloidal process, Int. J. Refract. Met. Hard Mater. 60 (2016) 68–74. https://doi.org/10.1016/j.ijrmhm.2016.07.010.

[10] W.G. Fahrenholtz, G.E. Hilmas, I.G. Talmy, J.A. Zaykoski, Refractory diborides of zirconium and hafnium, J. Am. Ceram. Soc. 90 (2007) 1347–1364. https://doi.org/10.1111/j.1551-2916.2007.01583.x.

[11] T.A. Parthasarathy, R.A. Rapp, M. Opeka, R.J. Kerans, A model for the oxidation of ZrB2, HfB2 and TiB2, Acta Mater. 55 (2007) 5999–6010. https://doi.org/10.1016/j.actamat.2007.07.027.

[12] L. Silvestroni, G. Meriggi, D. Sciti, Oxidation behavior of ZrB2 composites doped with various transition metal silicides, Corros. Sci. 83 (2014) 281–291. https://doi.org/10.1016/j.corsci.2014.02.026.

[13] L. Zoli, D. Sciti, Efficacy of a ZrB2???SiC matrix in protecting C fibers from oxidation in novel UHTCMC materials, Mater. Des. 113 (2017) 207–213. https://doi.org/10.1016/j.matdes.2016.09.104.

[14] A. Vinci, L. Zoli, E. Landi, D. Sciti, Oxidation behaviour of a continuous carbon fiber reinforced ZrB2–SiC composite, Corros. Sci. 123 (2017) 129–138. https://doi.org/10.1016/j.corsci.2017.04.012.

[15] W.G. Fahrenholtz, Thermodynamic analysis of ZrB2-SiC oxidation: Formation of a SiC-depleted region, J. Am. Ceram. Soc. 90 (2007) 143–148. https://doi.org/10.1111/j.1551-2916.2006.01329.x.

[16] P.A. Williams, R. Sakidja, J.H. Perepezko, P. Ritt, Oxidation of ZrB2-SiC ultra-high temperature composites over a wide range of SiC content, J. Eur. Ceram. Soc. 32 (2012) 3875–3883. https://doi.org/10.1016/j.jeurceramsoc.2012.05.021.

[17] A. Rezaie, W.G. Fahrenholtz, G.E. Hilmas, Evolution of structure during the oxidation of zirconium diboride-silicon carbide in air up to 1500°C, J. Eur. Ceram. Soc. 27 (2007) 2495–2501. https://doi.org/10.1016/j.jeurceramsoc.2006.10.012.

[18] A. Rezaie, W.G. Fahrenholtz, G.E. Hilmas, The effect of a graphite addition on oxidation of ZrB 2-

SiC in air at 1500??C, J. Eur. Ceram. Soc. 33 (2013) 413–421. https://doi.org/10.1016/j.jeurceramsoc.2012.09.016.

[19] F. Yang, X. Zhang, J. Han, S. Du, Processing and mechanical properties of short carbon fibers toughened zirconium diboride-based ceramics, Mater. Des. 29 (2008) 1817–1820. https://doi.org/10.1016/j.matdes.2008.03.011.

[20] F. Yang, X. Zhang, J. Han, S. Du, Characterization of hot-pressed short carbon fiber reinforced ZrB2-SiC ultra-high temperature ceramic composites, J. Alloys Compd. 472 (2009) 395–399. https://doi.org/10.1016/j.jallcom.2008.04.092.

[21] W. Hong, K. Gui, P. Hu, X. Zhang, S. Dong, Preparation and characterization of high-performance ZrB2--SiC--Cf composites sintered at 1450 {\textdegree}C, J. Adv. Ceram. 6 (2017) 110–119. https://doi.org/10.1007/s40145-017-0223-7.

[22] A. Vinci, L. Zoli, D. Sciti, C. Melandri, S. Guicciardi, Understanding the mechanical properties of novel UHTCMCs through random forest and regression tree analysis, Mater. Des. 145 (2018) 97–107. https://doi.org/10.1016/j.matdes.2018.02.061.

[23] L. Zoli, D. Sciti, Efficacy of a ZrB2–SiC matrix in protecting C fibers from oxidation in novel UHTCMC materials, Mater. Des. 113 (2017) 207–213. https://doi.org/10.1016/j.matdes.2016.09.104.

[24] A. Vinci, L. Zoli, D. Sciti, Influence of SiC content on the oxidation of carbon fiber reinforced ZrB2/SiC composites at 1500 and 1650 °C in air, J. Eur. Ceram. Soc. 38 (2018) 3767–3776. https://doi.org/10.1016/j.jeurceramsoc.2018.04.064.

[25] J. Han, P. Hu, X. Zhang, S. Meng, Oxidation behavior of zirconium diboride-silicon carbide at 1800 °C, Scr. Mater. 57 (2007) 825–828. https://doi.org/10.1016/j.scriptamat.2007.07.009.

[26] S.N. Karlsdottir, J.W. Halloran, Oxidation of ZrB 2-SiC: Influence of SiC content on solid and liquid oxide phase formation, J. Am. Ceram. Soc. 92 (2009) 481–486. https://doi.org/10.1111/j.1551-2916.2008.02874.x.

[27] H. Wu, W. Zhang, Fabrication and properties of ZrB2-SiC-BN machinable ceramics, J. Eur. Ceram. Soc. 30 (2010) 1035–1042. https://doi.org/10.1016/j.jeurceramsoc.2009.09.022.

[28] J. Han, P. Hu, X. Zhang, S. Meng, W. Han, Oxidation-resistant ZrB2-SiC composites at 2200 °C, Compos. Sci. Technol. 68 (2008) 799–806. https://doi.org/10.1016/j.compscitech.2007.08.017.

[29] S. Mungiguerra, G.D. Di Martino, A. Cecere, R. Savino, L. Silvestroni, A. Vinci, L. Zoli, D. Sciti, Arc-jet wind tunnel characterization of ultra-high-temperature ceramic matrix composites, Corros. Sci. 149 (2019) 18–28. https://doi.org/https://doi.org/10.1016/j.corsci.2018.12.039.

[30] S. Chen, C. Zhang, Y. Zhang, H. Hu, Preparation and properties of carbon fiber reinforced ZrC–ZrB2 based composites via reactive melt infiltration, Compos. Part B Eng. 60 (2014) 222–226. https://doi.org/10.1016/J.COMPOSITESB.2013.12.067.

[31] L. Liu, H. Li, W. Feng, X. Shi, K. Li, L. Guo, Ablation in different heat fluxes of C/C composites modified by ZrB2-ZrC and ZrB2-ZrC-SiC particles, Corros. Sci. 74 (2013) 159–167. https://doi.org/10.1016/j.corsci.2013.04.038.

[32] C. Sun, H. Li, Q. Fu, J. Zhang, Microstructure and ablation properties of carbon/carbon composites modified by ZrSiO4, Corros. Sci. 79 (2014) 100–107. https://doi.org/10.1016/j.corsci.2013.10.031.

[33] H. jun Li, X. yuan Yao, Y. lei Zhang, K. zhi Li, L. jun Guo, L. Liu, Effect of heat flux on ablation behaviour and mechanism of C/C-ZrB2-SiC composite under oxyacetylene torch flame, Corros. Sci. 74 (2013) 265–270. https://doi.org/10.1016/j.corsci.2013.04.052.

[34] A. Vinci, L. Zoli, D. Sciti, C. Melandri, S. Guicciardi, Understanding the mechanical properties of novel UHTCMCs through random forest and regression tree analysis, Mater. Des. 145 (2018). https://doi.org/10.1016/j.matdes.2018.02.061.

[35] D. Sciti, L. Silvestroni, F. Monteverde, A. Vinci, L. Zoli, Introduction to H2020 project C3HARME–next generation ceramic composites for combustion harsh environment and space, Adv. Appl. Ceram. (2018). https://doi.org/10.1080/17436753.2018.1509822.

[36] Y.-J. Lee, Formation of silicon carbide on carbon fibers by carbothermal reduction of silica, Diam. Relat. Mater. 13 (2004) 383–388. https://doi.org/10.1016/j.diamond.2003.11.062.

[37] M. Khoeini, A. Nemati, M. Zakeri, M. Tamizifar, H. Samadi, Comprehensive study on the effect of SiC and carbon additives on the pressureless sintering and microstructural and mechanical characteristics of new ultra-high temperature ZrB2 ceramics, Ceram. Int. 41 (2015) 11456–11463. https://doi.org/10.1016/j.ceramint.2015.05.110.

[38] S.S. Hwang, A.L. Vasiliev, N.P. Padture, Improved processing and oxidation-resistance of ZrB2 ultra-high temperature ceramics containing SiC nanodispersoids, Mater. Sci. Eng. A. 464 (2007) 216–224. https://doi.org/10.1016/j.msea.2007.03.002.

[39] L. Silvestroni, D. Dalle Fabbriche, C. Melandri, D. Sciti, Relationships between carbon fiber type and interfacial domain in ZrB2-based ceramics, J. Eur. Ceram. Soc. 36 (2016) 17–24. https://doi.org/10.1016/j.jeurceramsoc.2015.09.026.

[40] N. Jacobson, Oxidation and corrosion of ceramics and ceramic matrix composites, Curr. Opin. Solid State Mater. Sci. 5 (2001) 301–309. https://doi.org/10.1016/S1359-0286(01)00009-2.